1. Supplementary Notes

1.1. Supplementary Experimental Methods

Although Ub^{V76}-GFP having a half-life of a few minutes turned out to be the optimal choice for the final mammalian oscillator, we have used d2EYFP for initial proof-of-concept studies, but its half-life of 2h was not sufficiently short to enable robust oscillations (data not shown). In order to describe the iterative experimental-theoretical design process parts of these d2EYFP-based results have been included as controls in the Supplementary Information (see below). pBP282 (P_{hCMV*1}→d2EYFP) harbours a tetracycline-responsive d2EYFP expression unit, which is isogenic to the Ub^{V76}-GFP-encoding one of pMT100 ($P_{hCMV*-1}$→Ub^{V76}-GFP). Time-lapse microscopy of pBP282-containing CHO-K1 required a d2EYFP-specific excitation/emission filter set: d2EYFP (513/527nm; C/Y, Leica, cat. no. 11513897).

1.2. Structure of the First-Generation Mathematical Model

The aim of model development for the circuit was to elucidate whether – using known characteristics of the biological components – the system could establish a mammalian genetic oscillator, and which parameters would be critical for a more detailed design. For this purpose, we derived a semi-quantitative model based on ordinary differential equations (ODEs) to investigate design constraints and –parameters. Importantly, this approach allowed for integration of experimentally determined parameter values and, hence, for a realistic description of circuit function. At the same time, a qualitative analysis was enabled by a simplified mechanistic model that could be refined using quantitative experimental data.

Specifically, we established the model by considering the production and degradation of the two regulators (tTA and PIT) and GFP as well as the interactions between these components (summarized in Fig. 1b of the main text). Note that the initial mathematical model was developed for the reporter d2EYFP, and not Ub^{V76}-GFP used for the final oscillator and corresponding model (see below). The mathematical model, notably, has to describe all relevant time delays in the system because they are critical for oscillator performance. Hence, we considered transcription (denoted by *TC* in Fig. 1b of the main text) and translation (*TL*) processes individually, and included all corresponding degradation reactions (*D*). In addition, the time delay for forming active destabilized GFP (d2EYFP or Ub^{V76}-GFP) by protein folding is modelled explicitly.

The dynamics of the processes are described by a system of ODEs that considers the concentrations of the following components: tTA mRNA (T_m), tTA protein (T_p), PIT mRNA (P_m), PIT protein (P_p), tTA antisense mRNA (A_m), sense-antisense mRNA complex (TA_m), GFP mRNA (G_m), unfolded, inactive GFP protein (G_p), and active GFP (G_a). In addition, we use a short-hand notation, namely P1-P3, for the plasmids that carry tTA (P1; pMT35), PIT (P2; pMT36 or pMF156), and dGFP (P3; pBP282 or pMT100). The equations for the dynamic system were set up as follows:

$$\frac{dT_m}{dt} = G_1 \cdot r_T - k_1 \cdot A_m \cdot T_m + AT_m \cdot \left(k_2 + k_{DAm}\right) - k_{DTm} \cdot T_m \tag{1.1}$$

$$\frac{dT_p}{dt} = k_{TL} \cdot T_m - k_{DTp} \cdot T_p \tag{1.2}$$

$$\frac{dP_m}{dt} = G_2 \cdot r_T - k_{DPm} \cdot P_m \tag{1.3}$$

$$\frac{dP_p}{dt} = k_{TL} \cdot P_m - k_{DPp} \cdot P_p \tag{1.4}$$

$$\frac{dA_m}{dt} = G_1 \cdot r_P - k_1 \cdot A_m \cdot T_m + AT_m \cdot \left(k_2 + k_{DTm}\right) - k_{DAm} \cdot A_m \tag{1.5}$$

$$\frac{dAT_m}{dt} = k_1 \cdot A_m \cdot T_m - AT_m \cdot \left(k_2 + k_{DTm} + k_{DAm}\right) \tag{1.6}$$

$$\frac{dG_m}{dt} = G_3 \cdot r_T - k_{DGm} \cdot G_m \tag{1.7}$$

$$\frac{dG_p}{dt} = k_{TL} \cdot G_m - \left(k_3 + k_{DGp}\right) \cdot G_p \tag{1.8}$$

$$\frac{dG_a}{dt} = k_3 \cdot G_p - k_{DGp} \cdot G_a \tag{1.9}$$

To account for different dosage of the three plasmids P1-P3, the model employs parameters G_1 - G_3. The kinetics of gene expression are captured by rate laws r_T and r_P for tTA- and PIT-controlled transcription, respectively. Note that due to the particular kinetics of gene expression formulated by Eqs. (1.12) and (1.13) below, parameters G_1 - G_3 have the dimension of plasmids / cell.

Here, we capture the formation of the sense-antisense duplex in the negative feedback loop by mass-action (first-order) reaction kinetics with parameters k_1 for the association and k_2 for the dissociation processes, as applied previously for the description of oligonucleotide-mRNA interactions [30]. Furthermore, we assume that the degradation of the duplex is induced by decay of the individual RNA strands and that the influence of specific mechanisms for duplex recognition and degradation can be neglected. Degradation of mRNAs i and proteins j, in general, is modelled as first-order decay with parameters k_{Dim} and k_{Djp}, respectively. Also, general translation (parameter k_{TL}) and irreversible maturation of GFP by folding (parameter k_3) are simplified as first-order processes.

To model the effects of antibiotics as the control inputs for the system, one has to distinguish between active and inactive transcriptional activators. Consequently, we denote the concentrations of active transcriptional regulators tTA and PIT by T_a and P_a, respectively. They are proportional to the corresponding total protein concentrations (identified by subscripts p in the ODE system). A Michaelis-Menten-like inactivation rate law (see, e.g. experimental dose-response curves in [31]) captures the interactions between the regulators and the small molecules tetracycline, Tc, and pristinamycin I, PI, respectively:

$$T_a = T_p \cdot \left(1 - \frac{Tc}{K_{Mt} + Tc} \right) \tag{1.10}$$

$$P_a = P_p \cdot \left(1 - \frac{PI}{K_{Mp} + PI} \right) \tag{1.11}$$

To describe the rates of gene expression from tTA- and PIT-controlled promoters, we employ formal reaction rate laws typically used in synthetic biology [32] as simplified descriptions:

$$r_T = k_T \cdot \left(\alpha_T + (1 - \alpha_T) \cdot \frac{T_a^{n_T}}{K_{MT} + T_a^{n_T}} \right) \cdot f_V \tag{1.12}$$

$$r_P = k_P \cdot \left(\alpha_P + (1 - \alpha_P) \cdot \frac{P_a^{n_P}}{K_{MP} + P_a^{n_P}} \right) \cdot f_V \tag{1.13}$$

Here, the maximal rate constants k_T and k_P, respectively, are given in terms of the number of mRNA molecules transcribed per minute and gene copy. Basal transcriptional activities are

accounted for by the parameters α_T and α_P. Controlled gene expression follows Hill-type dose-response curves with promoter-activator affinities K_{MT} and K_{MP}, and cooperativity (Hill) coefficients n_T and n_P, respectively. Finally, the constant f_V accounts for the conversion of mRNA copy numbers to cellular mRNA concentrations in typical mammalian cells [33].

1.3. Initial Model Parametrization

For model parametrization, we relied on experimentally determined kinetic parameters and total protein concentrations from the literature as far as possible. To reduce the number of free parameters, we made the following simplifying assumptions:

i. Transfection efficiencies for all plasmids are equal and, thus, only the plasmid concentrations during transfection determine the cellular gene dosages.
ii. Degradation rates for tTA (sense and antisense), PIT, and dGFP mRNAs are similar.
iii. Maximal activation of gene expression by tTA and PIT is identical because both constructs share the same (VP16) transactivation domain [31].
iv. Translation rates are identical for all mRNAs. This assumption is already encoded in the model structure and based on the similar lengths of all proteins involved (in the range of 400-500 amino acids).
v. The affinities of tTA and PIT for their respective promoters can be approximated by average values from *in vitro* binding assays for TetR and Pip, which provide the DNA binding domains of the fused transactivators, respectively.

However, several of the model parameters had to be adjusted given experimentally supported ranges of possible parameter values (e.g., regarding protein and mRNA degradation time constants). For this adjustment, we employed Monte Carlo sampling in discretized parameter space to find a set of parameter values that yields oscillations of ~15h period. To constrain the search space to biologically meaningful values, we employed the following lower and upper bounds for parameter values: protein and mRNA half lives between 10 min and 180 min, plasmid concentration between 0 and 500 copies per cell for 50 ng/ml DNA provided during transfection [34], sense-antisense mRNA association constant between 10^{-2} and 10^{2} μM^{-1} min^{-1} [30], and translation / transcription rates between 10^{-2} and 10^{2} min^{-1}. Supplementary Table 1 lists all these reference parameter values, including their description, references for specific parameters, and calculation methods for inferred values.

1.4. Parameter Estimation

For refinement of the model according to the experimentally observed circuit behaviour, we next estimated several of the model parameters from experimental data shown in Fig. 2 of the main text (see Supplementary Table 2 for details). Kinetic parameters and gene doses were estimated with an evolutionary strategy [35] according to a combined minimization criterion constructed by:

$$\min\ \boldsymbol{\theta} \rightarrow \sum_j \left(\frac{x_j^m - x_j^c(\boldsymbol{\theta})}{\delta_j} \right)^2 + w_O \cdot \sum_{i \in E_O} \Phi_O(\boldsymbol{\theta}, i) + w_S \cdot \sum_{i \in E_S} \Phi_S(\boldsymbol{\theta}, i) \qquad (1.14)$$

The optimization routine searches for a set of parameters $\boldsymbol{\theta}$ that minimizes the objective function on the right-hand side. The first term of the objective function defines a weighted least-squares error, where j is the index for the data points, $\mathbf{x^c}$ are the calculated state variables of the ODE model, $\mathbf{x^m}$ is the vector of experimental data, and δ_j is the corresponding measurement variance. To avoid overfitting of data points with concentrations close to zero, we determined the effective measurement variance as $\delta_j = max(0.5 \cdot x^m_j, 0.5)$, assuming a high variance of 50% in the experimental data (accounting for cell-to-cell variability) and a lower detection level of ~0.5 relative fluorescence units.

The second and third term of Eq. (1.14) take into account the system's qualitative behaviour. They 'punish' steady-state behaviour when the system is observed to oscillate in an experiment (set E_O for the indices of the corresponding experiments), and oscillations when it should approach steady-state (set E_S), respectively. Parameters w_O and w_S serve to weigh these contributions. The functionals $\Phi_O(\boldsymbol{\theta}, i)$ and $\Phi_S(\boldsymbol{\theta}, i)$ are defined as:

$$\Phi_O(\boldsymbol{\theta}, i) = \begin{cases} 0 & \text{if oscillations in model and experiment} \\ 1 & \text{if oscillatory behavior does not agree} \end{cases} \qquad (1.15)$$

$$\Phi_S(\boldsymbol{\theta}, i) = \begin{cases} 0 & \text{if steady-state in model and experiment} \\ 1 & \text{if steady-state behavior does not agree} \end{cases} \qquad (1.16)$$

Here, we adjusted the weights to $w_O = w_S = 10$. Note that unlike gradient-based optimization methods, evolutionary algorithms are not strictly dependent on the quality of the starting points and are robust for solving non-linear problems [35]. The experimental data used for parameter estimation are compiled in Supplementary Table 2.

In estimating the parameter values, however, we found that when assuming simultaneous DNA uptake by all cells (at the same, estimated time point after start of the transfection), the model could not describe the experimental data (see Supplementary Fig. 1). The timing of plasmid uptake essentially is a random process because the cells are not synchronized in their

cell cycle and become competent for transfection at different time points. Therefore, in addition, we estimated times of transfection for each individual cell (included in Supplementary Table 2). Supplementary Table 3 provides the resulting parameter values that apply to all experiments with and without variable transfection times.

As an independent test for plausibility of the estimated kinetic parameters, we considered the case of stable chromosomal integration of a tTA-controlled GFP in CHO-K1 cells, for which an average steady-state value of 244 mRNA molecules per transcriptionally active cell was measured [36]. For the mathematical model, the expected steady-state value for this scenario (full activity of tTA-controlled gene expression) can be calculated as:

$$G_m^{ss} = \frac{k_T}{k_{DGm}} \approx 616 \text{ mRNA molecules / cell} \tag{1.17}$$

Hence, with the estimated parameter values, the same order of magnitude for the steady-state mRNA concentration is obtained.

1.5. Analysis of Single-Cell Data

For detailed statistical analysis of the circuit behaviour based on single-cell data, we devised computational methods for (i) model-based alignment of single-cell fluorescence trajectories for non-oscillating cells (e.g., for control cells cultivated in the presence of antibiotics), and (ii) unbiased estimation of oscillator period and amplitude from noisy single-cell data. In both areas, the methods yielded estimates of cell-to-cell variability that were used for adjustment of the refined mathematical model (see section 1.6) and for analysis of oscillator performance.

For control experiments, variability of, for instance, reporter gene induction profiles could be related to different timing of plasmid uptake, divergent plasmid doses in individual cell, or other stochastic effects. To dissect such contributions, we employed simplified mathematical models to approximate induction or repression time-courses. Time-courses of increasing fluorescence for an individual cell *i, $F_i(t)$,* were described by:

$$F_i(t) = \begin{cases} F_{\max} \cdot \left(1 - \exp(\lambda(t - \Delta t_i)\right) & \text{for } t > \Delta t_i \\ 0 & \text{for } t \le \Delta t_i \end{cases} \tag{1.18}$$

with maximal fluorescence signal F_{max} , time constant λ, and time delay for plasmid uptake in the respective cell, Δt_i. We determined model parameters by maximum likelihood estimation for a sample of individual cells using an evolutionary strategy (in analogy to parameter estimation described in section 1.4). Effectively, this lead to an alignment of single-cell trajectories because only the time delays were specific for each cell, while the maximal fluorescence and the time constant were identical for all cells.

Similarly, we employed a first-order decay model for data alignment at decreasing fluorescence over time (e.g., in tetracycline-treated cultures):

$$F_i'(t) = \begin{cases} F_{\max} \cdot \exp(-\lambda(t - \Delta t_i)) & \text{for } t > \Delta t_i \\ F_{\max} & \text{for } t \le \Delta t_i \end{cases}. \quad (1.19)$$

with maximal fluorescence signal F_{max}, time constant λ, and time delay Δt_i for plasmid uptake by cell i. We used a stochastic optimization algorithm (see section 1.4) to estimate the free parameters in the above models, using a maximum likelihood estimation over all experimental data sets.

The corresponding aligned single-cell trajectories for non-oscillating control experiments are shown in Supplementary Fig. 4. In all cases, the experimental and modelling data aligned well, indicating that variable timing of plasmid uptake is a major source of cell-to-cell variability in the observed behaviours. In contrast, the variation of fluorescence intensities for the aligned experimental data was on the order of 20%, which suggests that – at least for the non-oscillating controls – variations in plasmid number and other cellular parameters have a low impact on the quantitative behaviour.

In addition, our model-based data analysis suggested that in the control experiments involving engineered cells cultivated in the presence of tetracycline, oscillations might occur before an effective shut-down of the gene expression system (Supplementary Fig. 4e,f). This is consistent with prior observations of a substantial time-delay between addition of the antibiotic to the culture medium and complete suppression of gene expression [37]. Note that in the above experiments, fluorescence recording started 6h after addition of tetracycline. We therefore conducted another control experiment with simultaneous addition of the drug and start of recording. For some cells, 1-2 oscillations could be observed even after tetracycline addition (Supplementary Fig. 5). This confirmed an effective time-delay between drug addition and effects on gene expression, which was considered in further model refinement (see below).

Another technical challenge in data analysis concerned the exact, unbiased determination of oscillator period and amplitude from noisy single-cell fluorescence time-courses. For each cell, we first extracted tails of zero-concentration at both the beginning and the end of the recorded GFP intensity profiles. We subsequently smoothed the time-course to avoid capturing information on local maxima or minima that would bias the measurement of the driving oscillation. For this purpose, we used the Matlab function *filter* and obtained the running average of the vector containing the time-varying GFP intensities, using a window size of 4 time points. Next, we applied a Fast Fourier Transform to the smoothed data and

obtained the real-valued one-sided power-spectral density profile of the GFP intensities, from where the index related to the maximum was identified and the period of the driving oscillation was obtained by its direct relation to the maximal spectral power. Each GFP time-course exhibiting sustained oscillations was then partitioned into windows of size equal to the computed period, starting from their first oscillation maximum. Next, we recorded the amplitude in each window as the difference between the maximal and minimal fluorescence discarding amplitudes smaller than 15% of the maximal amplitude length on the grounds of probable noise, finally obtaining an average amplitude and period for each cell. Once the data for all cells corresponding to the same plasmid transfection dosage were gathered, cells with periods smaller than 5% of the length of the largest recorded period were discarded, and a mean period and amplitude for each dosage was obtained, along with their corresponding standard deviations.

This method was applied to both experimental (single-cell data for Ub^{V76}-GFP reporter constructs) and *in silico* results, obtaining mean periods and amplitudes for each dosage. The method's accuracy was verified upon comparison with an interactive application in which the maxima and minima of the oscillations were selected manually from the experimental GFP time-courses and 'exact' periods and amplitudes were obtained. Hence, the method optimization came down to selecting an appropriate window size for the smoothing algorithm as well as percentages of discarded periods and amplitudes. Among window sizes varying from 2 to 20 time points, the running average widow size of 4 resulted in optimal data fitting. Similarly, discarding amplitudes smaller than 15% of the maximal amplitude length and periods smaller than 5% of the maximal period length resulted optimal, among percentages varying from 2% to 50% for each case.

1.6. Refined Mathematical Model and Stochastic Analysis

As suggested by the experimental data analysis, a more realistic mathematical model that could be adapted quantitatively to the experimental data needed to cover more biological detail (e.g. regarding the time-delay between tetracycline addition and effect) as well as cell-to-cell variability. In particular, intrinsic noise is central to genetic regulatory networks and their accurate modelling. It stems from the uncertainty of knowing when a reaction will occur and which reaction type it will be. Naturally, this is more likely to be observed in systems where there are small to moderate molecular concentrations. However, it should be noted that systems with large molecular concentrations are not exempt of displaying effects of internal noise. Our experimental findings show that the amplitudes and periods of active GFP

fluorescence intensity are far from being uniform and we hypothesize the variation stems from internal noise. Hence, we opted for obtaining stochastic simulations that take proper account of intrinsic randomness.

In a first step towards a full stochastic model, we modified the deterministic model (section 1.2) by including additional detail on the action of tetracycline and on the central sense-antisense expression unit (pMT35). The former modifications were induced by the experimentally observed time-delays (see above), while the latter modifications proved necessary to enable a quantitative description of all experimental data (data not shown).

More specifically, we modelled the time-delay for tetracycline by distinguishing between external (Tc^{ext}) and internal (Tc) tetracycline concentrations and by connecting both through a temporally simplified diffusion process:

$$\frac{dTc}{dt} = k_{DTc} \cdot \left(Tc^{ext} - Tc \right) \tag{1.20}$$

In this way, Tc became an additional dynamic state of the model that is connected to the input concentration via the temporally simplified diffusion constant k_{DTc}.

Model adjustment to the experimental data, in addition, required more substantial modification of the model with respect to the representation of the sense-antisense construct. The basic processes considered in this modification are sketched in Supplementary Fig. 6. We assume that interactions between concurrent transcriptional activities of the sense and antisense strands take place in a single location on the DNA. The two corresponding compartments are designated X_s and X_a for the sense and antisense strands, respectively. Their locations relative to the promoters are defined by a free (scaled) parameter α. To model interactions between the transcriptional units, we assume that occupancy of X_a with RNA polymerase increases the probability that transcription of the sense strand will abort prematurely. With probability β, transcripts of the sense strand will complete and, thus, lead to functional mRNA. Here, β depends on the occupancy of X_a as well as on additional model parameters. Note that, in this setting, non-functional sense mRNAs do not need to be tracked because they cannot form active tTA proteins, and that the interaction between the strands is not symmetric: short antisense mRNAs (of relative length 1-α) could still be functional in terms of repressing sense mRNA translation.

Translation of this concept into dynamic equations for the sense-antisense gene expression unit leads to two ODEs that replace Eqs. (1.1) and (1.5) of the original model, respectively:

$$\frac{dT_m}{dt} = \frac{k_T}{1-\alpha} \cdot \beta \cdot X_s - k_1 \cdot A_m \cdot T_m + AT_m \cdot \left(k_2 + k_{DAm} \right) - k_{DTm} \cdot T_m \tag{1.21}$$

$$\frac{dA_m}{dt} = \frac{k_T}{\alpha} \cdot X_a - k_1 \cdot A_m \cdot T_m + AT_m \cdot \left(k_2 + k_{DTm}\right) - k_{DAm} \cdot A_m \tag{1.22}$$

We assume a simple Michaelis-Menten type saturating function for probability β, namely:

$$\beta = \frac{k_{IAS}}{k_{IAS} + X_a / G_1} \cdot \tag{1.23}$$

where k_{IAS} is a parameter that captures the effective inhibition of sense by antisense transcription. The dynamic equations for the intermediary DNA compartments are given by:

$$\frac{dX_s}{dt} = G_1 \cdot r_T \cdot \frac{\varphi_s}{\alpha} - \frac{k_T}{1-\alpha} \cdot X_s \tag{1.24}$$

$$\frac{dX_a}{dt} = G_1 \cdot r_P \cdot \frac{\varphi_a}{1-\alpha} - \frac{k_T}{\alpha} \cdot X_a. \tag{1.25}$$

The two functions φ_a and φ_s, finally, account for the fact that the intermediary compartments cannot have higher occupancies than allowed by the total gene dosage. Again, we employ simple saturating kinetics for their formal definition:

$$\varphi_s = \frac{1 - X_s / G_1}{1 + k_{MTC} - X_s / G_1} \quad , \quad \varphi_a = \frac{1 - X_a / G_1}{1 + k_{MTC} - X_a / G_1} \tag{1.26}$$

with an apparent affinity constant k_{MTC} for transcriptional elongation. Apparently, the functions defined in Eqs. (1.23) and (1.26) are only well-behaved for $G_1 \neq 0$; we set the corresponding values to zero when the plasmid was absent.

For parameter estimation of the refined model, we employed the strategy as described in section 1.4, and employed the aligned single-cell data as well as the corresponding experimental standard deviations (see section 1.5). The corresponding estimated parameter values are summarized in Supplementary Table 4; note that most of these model parameters are close to the literature values or estimated values for the first-generation model. The resulting model behaviours for controls and oscillating regimes as well as the experimental data used for parameter estimation are shown in Supplementary Fig. 7.

However, intrinsic noise and delays are central to oscillating patterns of gene expression [38]. Intrinsic noise stems from the uncertainty of knowing when a reaction will occur and which reaction type it will be. Delays, on the other hand, are intrinsic to slow biochemical processes that do not occur instantaneously and are often affected by spatial heterogeneities. There are multiple stochastic methods tailored to address diverse modelling issues, where one has to decide to either explicitly account for spatiotemporal steps [39] or opt for a much faster temporally-resolved stochastic solver [40]. Such decision is generally based on the scales of

reaction and diffusion processes, whether there are strong indications of sustained spatial heterogeneity and, finally, the desired time-span of analysis.

In the stochastic version of the model, we assumed all components to be well-mixed, opting for a temporally-resolved approach. Given the high molecular concentrations considered in this oscillator, we needed to coarse-grain the simulation in time. For all stochastic simulations we used the Bτ-DSSA [40], an algorithm that has been shown to accurately capture the dynamics of molecular clocks in extremely reduced CPU times. The Bτ-DSSA is a new generalized Binomial τ-leap method that addresses previous difficulties associated with complex chemical kinetics in coarse-grain methods, and introduces delays into the Binomial τ-leap framework in multi-cellular settings. Specific parameters used in Bτ-DSSA were an epsilon of 0.01 and uniform time ticks separated by one minute. One should note that the latter is solely for presentation purposes and differs from the simulator time-stepping, which depends on the reaction propensities and in most cases yields inhomogeneous time steps.

The dynamics of the molecular processes involve the exact same components used in the deterministic model, whereas the corresponding chemical reactions are summarized by Supplementary Table 5.

In order to study how plasmid concentrations affect the driving oscillation, we performed stochastic simulations with plasmids pMT35, pMT36 and pBP282 (1:1:1), ranging between 40 and 350 ng DNA/500µl culture volume. For each dosage we obtained 20 independent simulations in a 'real-time' span of 1500 minutes. Such simulations in turn yielded the GFP intensities from which final periods and amplitudes were obtained. The stochastic model provided counter-intuitive predictions regarding the impact of molecular noise on the share of oscillating cells (Supplementary Fig. 8) and on noise-induced oscillations at gene dosages where no oscillations are observed in the deterministic regime (Supplementary Fig. 9).

1.7. Supplementary References

30 C. M. Roth, *Biophys J* **89** (4), 2286 (2005).

31 M. Fussenegger, R. P. Morris, C. Fux et al., *Nat Biotechnol* **18** (11), 1203 (2000).

32 M. Kaern, W. J. Blake, and J. J. Collins, *Annu Rev Biomed Eng* **5**, 179 (2003).

33 W. Weber, J. Stelling, M. Rimann et al., *Proc Natl Acad Sci U S A* **104** (8), 2643 (2007).

34 P. Batard, M. Jordan, and F. Wurm, *Gene* **270** (1-2), 61 (2001).

35 C. G. Moles, P. Mendes, and J. R. Banga, *Genome Res* **13** (11), 2467 (2003).

36 A. Raj, C. S. Peskin, D. Tranchina et al., *PLoS Biol* **4** (10), e309 (2006).

[37] M. Gossen and H. Bujard, *Proc Natl Acad Sci U S A* **89** (12), 5547 (1992).

[38] M. Barrio, K. Burrage, A. Leier et al., *PLoS computational biology* **2** (9), e117 (2006); N. A. Monk, *Curr Biol* **13** (16), 1409 (2003).

[39] T. T. Marquez-Lago and K. Burrage, *The Journal of chemical physics* **127** (10), 104101 (2007).

[40] A. Leier, T. T. Marquez-Lago, and K. Burrage, *The Journal of chemical physics* **128** (20), 205107 (2008).

[41] M. Takahashi, L. Altschmied, and W. Hillen, *J Mol Biol* **187** (3), 341 (1986).

[42] M. Folcher, R. P. Morris, G. Dale et al., *J Biol Chem* **276** (2), 1479 (2001).

[43] A. Kamionka, J. Bogdanska-Urbaniak, O. Scholz et al., *Nucleic Acids Res* **32** (2), 842 (2004).

[44] L. Malphettes and M. Fussenegger, *Metab Eng* **8** (6), 672 (2006).

[45] S. P. Walton, G. N. Stephanopoulos, M. L. Yarmush et al., *Biophys J* **82** (1 Pt 1), 366 (2002).

[46] A. Gordon, A. Colman-Lerner, T. E. Chin et al., *Nat Methods* **4** (2), 175 (2007).

[47] X. Li, X. Zhao, Y. Fang et al., *J Biol Chem* **273** (52), 34970 (1998).

2. Supplementary Tables

Supplementary Table 1: Reference parameter values for the mammalian oscillator model.

Para-meter	Description	Value	Comments / Reference
G_1	Gene dosage plasmid 1	100	Calculated from experimental data [34] *
G_2	Gene dosage plasmid 2	100	Identical to value of G_1.
G_3	Gene dosage plasmid 3	100	Identical to value of G_1.
K_{Mt}	Affinity tet–tTA interaction	1.0 nM	Literature data [41]
K_{Mp}	Affinity pris–PIT interaction	1000 nM	Literature data [42]
k_T	Maximal transcription tTA-controlled promoter	30 min^{-1}	Adjusted by MC sampling.
k_P	Maximal transcription PIT-controlled promoter	30 min^{-1}	Identical to value for tTA-controlled transcription.
α_T	Basal activity of tTA-controlled promoter	0.085	Literature data [31] **
α_P	Basal activity of PIT-controlled promoter	0.056	Literature data [31] **
K_{MT}	Affinity tTA-binding to promoter	3.0 nM	Average affinity tetR / Pip [42,43]
K_{MP}	Affinity PIT-binding to promoter	3.0 nM	Identical to value for tTA.
n_T	Cooperativity for tTA-controlled gene expression	2.0	Literature data [44]
n_P	Cooperativity for PIT-controlled gene expression	2.0	Literature data [42]
K_1	Association tTA sense-antisense complex	4 μM^{-1} min^{-1}	Based on antisense oligonucleotides [30,45]
K_2	Dissociation tTA sense-antisense complex	0.001 min^{-1}	Based on antisense oligonucleotides [30,45]
K_3	Folding rate GFP	0.0154 min^{-1}	Average fluorophore formation rate [46].
K_{DTm}	Degradation rate tTA sense mRNA	0.0173 min^{-1}	Adjusted by MC sampling (half-life of 40 min).
K_{DAm}	Degradation rate tTA antisense mRNA	0.0173 min^{-1}	Identical to value of K_{DTm}.
K_{DPm}	Degradation rate PIT mRNA	0.0173 min^{-1}	Identical to value of K_{DTm}.
K_{DGm}	Degradation rate GFP mRNA	0.0173 min^{-1}	Identical to value of K_{DTm}.
k_{TL}	General translation rate	0.02 min^{-1}	Adjusted by MC sampling.
K_{DTp}	Degradation rate tTA protein	0.0231 min^{-1}	Adjusted by MC sampling (half-life of 30 min).
K_{DPp}	Degradation rate PIT protein	0.0658 min^{-1}	Calculated from gene expression ratios [31] ***.
K_{DGp}	Degradation rate GFP protein	0.0058 min^{-1}	Half-life of destabilized GFP ~ 2h [47].
f_V	Concentration scaling factor for copies / cell	$1.85 \cdot 10^{-3}$ nM	Calculated from average volume of CHO cells [33]

* Calculated from ~10'000 – 30'000 plasmid copies detected in 50% of CHO cells after transfection with 2'500 ng/ml DNA, and assuming that ~10% of the plasmids are nuclear and, thus, transcriptionally active.
** Calculated from relative levels of tTA- and PIT-controlled protein expression in CHO cells with and without saturating concentrations of transactivators and antibiotics.
*** Calculated from relative levels of maximal tTA- and PIT-controlled protein expression in CHO cells, assuming that protein degradation is the main contributing factor for the observed ratio of ~3.8 for the Tet-Off vs. the Pip-Off system.

Supplementary Table 2: Fluorescence measurements used for parameter estimation and estimated transfection times. All fluorescence data are in relative units; times refer to the start of recording the GFP signal (GFP) and of the experiment (transfection), respectively. When we assumed simultaneous DNA uptake by all cells, we estimated a transfection time of 441 min.

Experiment (Figure #)	GFP at t=0 min	GFP at t=450 min	GFP at t=900 min	Transfection time [min]
2a	0.8	4.4	9.4	597
2b	0.0	4.2	11.0	738
2c	3.5	0.5	0.5	0
2d	0.3	0.3	0.3	0
2e	9.8	9.0	6.4	150
2f	6.4	9.4	8.4	462
2g	2.5	0.8	1.8	0

Supplementary Table 3: Parameter values estimated from experimental data. Reference values refer to the parameters listed in Supplementary Table 1.

Para-meter	Description	Reference	Estimated w/o var. transfection	Estimated with var. transfection	Comments / Reference
G_1	Gene dosage plasmid 1	100	108	110	
G_2	Gene dosage plasmid 2	100	108	110	Identical to G_1.
G_3	Gene dosage plasmid 3	100	108	110	Identical to G_1.
k_T	Maximal transcription tTA-controlled promoter	30 min^{-1}	6.06 min^{-1}	6.47 min^{-1}	
k_P	Maximal transcription PIT-controlled promoter	30 min^{-1}	6.06 min^{-1}	6.47 min^{-1}	Identical to k_T.
K_1	Association tTA sense-antisense complex	4 μM^{-1} min^{-1}	10 μM^{-1} min^{-1}	10 μM^{-1} min^{-1}	
K_{DTm}	Degradation tTA sense mRNA	0.0173 min^{-1}	0.0102 min^{-1}	0.0105 min^{-1}	
K_{DAm}	Degradation tTA antisense	0.0173 min^{-1}	0.0102 min^{-1}	0.0105 min^{-1}	Identical to K_{DTm}.
K_{DPm}	Degradation rate PIT mRNA	0.0173 min^{-1}	0.0102 min^{-1}	0.0105 min^{-1}	Identical to K_{DTm}.
K_{DGm}	Degradation rate GFP mRNA	0.0173 min^{-1}	0.0102 min^{-1}	0.0105 min^{-1}	Identical to K_{DTm}.
k_{TL}	General translation rate	0.0200 min^{-1}	0.0422 min^{-1}	0.0526 min^{-1}	
K_{DTp}	Degradation rate tTA protein	0.0231 min^{-1}	0.0228 min^{-1}	0.0203 min^{-1}	
K_{DPp}	Degradation rate PIT protein	0.0658 min^{-1}	0.0693 min^{-1}	0.0693 min^{-1}	Calculated as above.
f_F	Conversion factor GFP concentrations – relative fluorescence units	N/A	10.44 μM^{-1}	7.93 μM^{-1}	

Supplementary Table 4: Estimated parameter for the refined oscillator model.

Para-meter	Description	Value	Comments / Reference
G_1	Gene dosage plasmid 1	131	Estimated.
G_2	Gene dosage plasmid 2	131	Identical to value of G_1.
G_3	Gene dosage plasmid 3	131	Identical to value of G_1.
K_{Mt}	Affinity tet–tTA interaction	0.6 nM	Estimated.
K_{Mp}	Affinity pris–PIT interaction	640 nM	Estimated.
k_T	Maximal transcription tTA-controlled promoter	2.81 min^{-1}	Estimated.
k_P	Maximal transcription PIT-controlled promoter	1.52 min^{-1}	Estimated.
α_T	Basal activity of tTA-controlled promoter	0.02	Estimated.
α_P	Basal activity of PIT-controlled promoter	0.02	Estimated.
K_{MT}	Affinity tTA-binding to promoter	1.0 nM	Estimated.
K_{MP}	Affinity PIT-binding to promoter	1.3 nM	Estimated.
n_T	Cooperativity for tTA-controlled gene expression	1.88	Estimated.
n_P	Cooperativity for PIT-controlled gene expression	2.75	Estimated.
K_1	Association tTA sense-antisense complex	431 μM^{-1} min^{-1}	Estimated.
K_2	Dissociation tTA sense-antisense complex	0.0002 min^{-1}	Estimated.
K_3	Folding rate dGFP	0.90 min^{-1}	Estimated.
K_{DTm}	Degradation rate tTA sense mRNA	0.0126 min^{-1}	Estimated.
K_{DAm}	Degradation rate tTA antisense mRNA	0.0365 min^{-1}	Estimated.
K_{DPm}	Degradation rate PIT mRNA	0.0437 min^{-1}	Estimated.
K_{DGm}	Degradation rate GFP mRNA	0.0609 min^{-1}	Estimated.
k_{TL}	General translation rate	1.453 min^{-1}	Estimated.
K_{DTp}	Degradation rate tTA protein	0.0553 min^{-1}	Estimated.
K_{DPp}	Degradation rate PIT protein	0.0955 min^{-1}	Estimated.
K_{DGp}	Degradation rate GFP protein	0.0775 min^{-1}	Estimated.
f_V	Concentration scaling factor for copies / cell	$1.85 \cdot 10^{-3}$ nM	Calculated as above.
f_F	Conversion factor for relative fluorescence units	15.01 μM^{-1}	Estimated.
k_{DTc}	Diffusion constant tetracycline	0.0012 min^{-1}	Estimated.
A	Relative location of sense-antisense interference	0.883	Estimated.
k_{IAS}	Inhibition constant sense-antisense	0.997	Estimated.
k_{MTC}	Apparent saturation transcriptional elongation	0.001	Estimated.

Supplementary Table 5: Reactions, reaction types and associated kinetic parameters for the stochastic model.

Reaction	Type	Parameters
Gm → 0	Degradation	K_{DGm}
Gm → Gm + Gp	Non-consuming unary	k_{TL}
Gp → 0	Degradation	K_{DGp}
Ga → 0	Degradation	K_{DGp}
Gp → Ga	Unary	K_3
(Tp + G3) → (Tp + G3) + Gm	Hill-type (r_T)	k_T
Tp → 0	Degradation	K_{DTp}
Tm → Tm + Tp	Non-consuming unary	k_{TL}
Xs → Xs + Tm	β function	$k_T / (1-\alpha)$
Tm + Am → ATm	Binary	k_1
ATm → Am + Tm	Unary	k_2
ATm → Tm	Degradation of Am	K_{DAm}
ATm → Am	Degradation of Tm	K_{DTm}
Tm → 0	Degradation	K_{DTm}
Xa → Am	Unary	k_T / α
Am → 0	Degradation	K_{DAm}
Pm → 0	Degradation	K_{DPm}
Pm → Pm + Pp	Non-consuming unary	k_{TL}
Pp → 0	Degradation	K_{DPp}
(Tp + G2) → (Tp + G2) + Pm	Hill-type (r_T)	k_T
(Tp + G1) → (Tp + G1) + Xs	Hill-type ($r_T \cdot \varphi_S$)	k_T / α
(Pp + G1) → (Pp + G1) + Xa	Hill-type ($r_P \cdot \varphi_A$)	$k_P / (1-\alpha)$
Tc → 0	Degradation	k_{DTc}
Xs → 0	Degradation	$k_T / (1-\alpha)$

3. Supplementary Figures

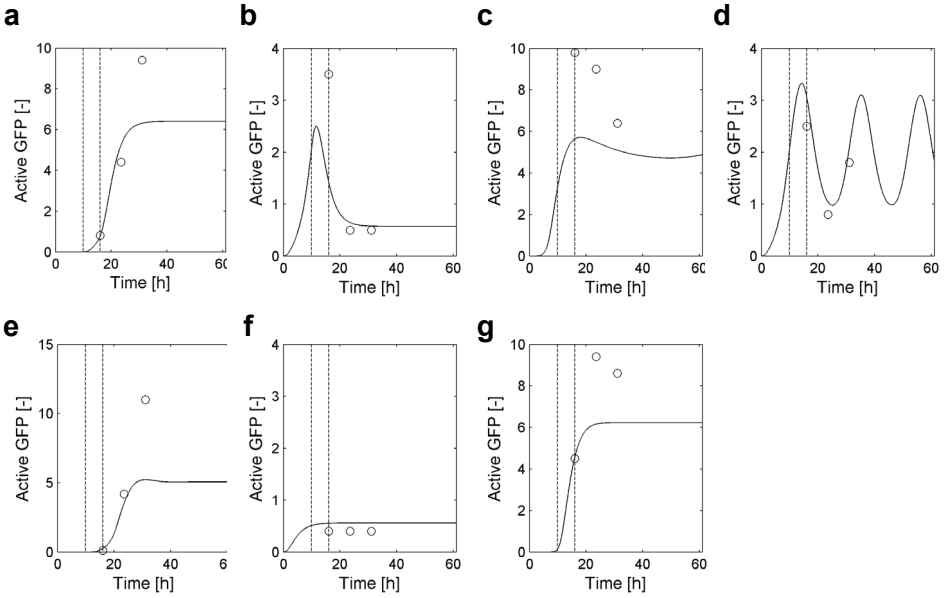

Supplementary Figure 1: Predictions of the adapted model with variable transfection times. Systems behaviour for different plasmid combinations and treatments with antibiotics (input signals) where cells are transfected with plasmids at t = 0h, antibiotics are added 10h after transfection (left dashed line), and recording of GFP signals starts 16 h after transfection (right dashed line). Solid lines are simulation results and circles denote selected experimental data for: (**a**) CHO-K1 co-transfected with pMT35 ($P_{hCMV*-1}$→tTA←P_{PIR}) and pBP282 ($P_{hCMV*-1}$→d2EYFP) (1:1; no antibiotics), (**b**) pMT35, pMT36 ($P_{hCMV*-1}$→PIT), pBP282 (1:1:1; 1ng/500µl tetracycline), (**c**) pMT35, pMT36, pBP282 (2:1:1; no antibiotics), (**d**) pMT35, pMT36, pBP282 (1:1:1; no antibiotics), (**e**) pMT35, pMT36, pBP282 (1:1:1; 200ng/500µl pristinamycin I added 10h after transfection), (**f**) pMT35, pMF156 (P_{hCMV}-PIT), pBP282 (1:1:1; no antibiotics), (**g**) pMT35, pMT36, pBP282 (3:1:1; no antibiotics).

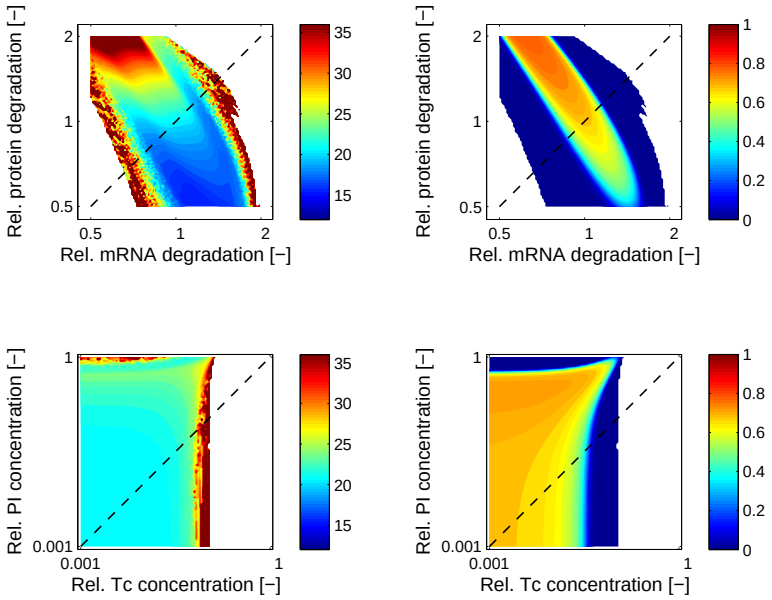

Supplementary Figure 2: Predicted systems behaviour depending on model parameters and inputs. Panels show the colour-coded oscillator period (left panels, period duration in hours indicated by the colour bar) and normalized amplitude (right panels) as a function of parameters and inputs in analogy to Fig. 2. (**a**,**b**) System performance as a function of relative mRNA (all mRNAs) and protein (all proteins except GFP) degradation parameters. (**c**,**d**) Effect of tetracycline (Tc) and pristinamycin I (PI) addition; concentrations are relative to doses for experiments shown in Supplementary Fig. 1.

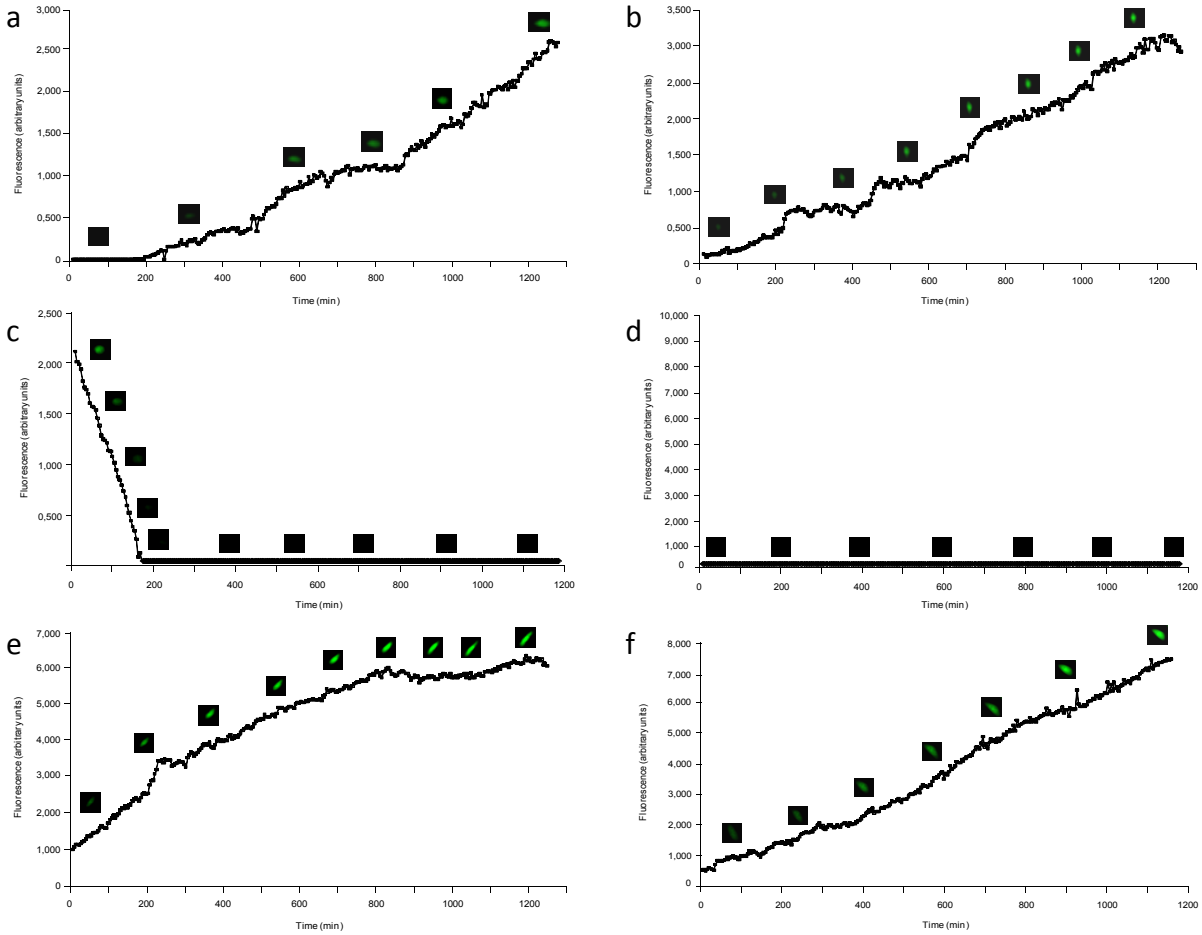

Supplementary Figure 3: Validation of mammalian oscillator components and systems behaviour by time-lapse fluorescence analysis of transfected CHO-K1. For each system set-up two independent fluorescence profiles of two different cells are shown. (**a**) CHO-K1 co-transfected with pMT35 ($P_{hCMV*-1}$→tTA←P_{PIR}) and pMT100 ($P_{hCMV*-1}$-Ub^{V76}-GFP) (1:1; no antibiotics), (**b**) pMT35, pMT36 ($P_{hCMV*-1}$→PIT), pMT100 (1:1:1; 200ng/500µl pristinamycin I added 10h after transfection), (**c**) pMT35, pMT36, pMT100 (1:1:1; 1ng/500µl tetracycline added 10h after transfection), (**d**) pMT35, pMF156 (P_{hCMV}-PIT), pMT100 (1:1:1; no antibiotics), (**e**) pMT35, pMT36, pMT100 (2:1:1; no antibiotics), (**f**) pMT35, pMT36, pMT100 (3:1:1; no antibiotics).

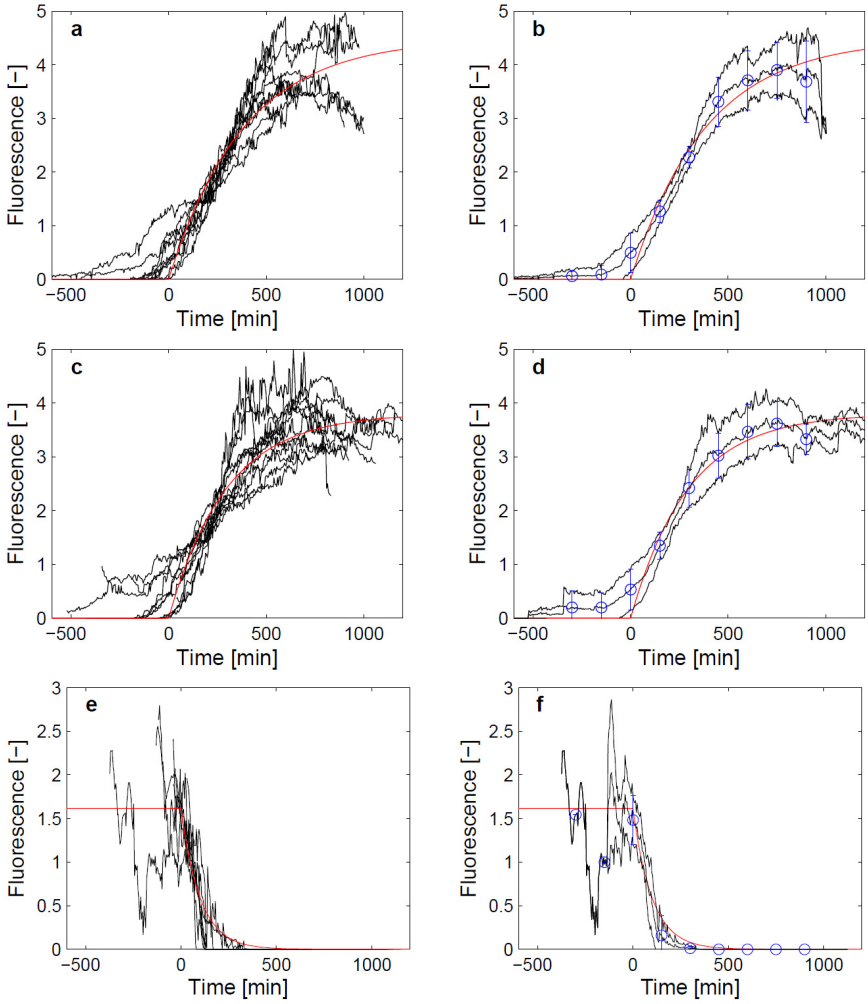

Supplementary Figure 4: Model-based alignment of single-cell trajectories. **a.** Aligned fluorescence signals (black) and model (red) with transfection times adjusted to t = 0 min for the two-plasmid control. **b.** Two-plasmid control with model (red), signal average and standard deviations for the entire time-course (black) and for selected time-points used in parameter estimation for the refined model (blue). Corresponding data analysis for control experiments with pristinamycin (**c,d**) and tetracycline (**e,f**) addition.

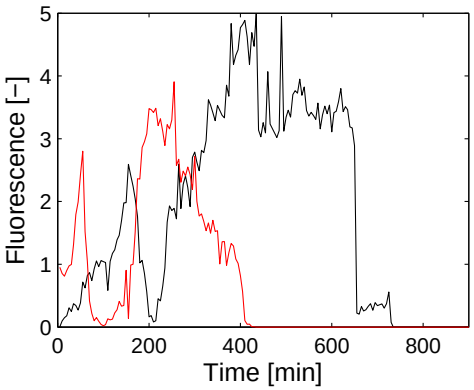

Supplementary Figure 5: Example single-cell trajectories for control experiments with simultaneous addition of tetracycline and start of fluorescence recording at t = 0 min. All other experimental settings correspond to those for Supplementary Fig. 4e,f.

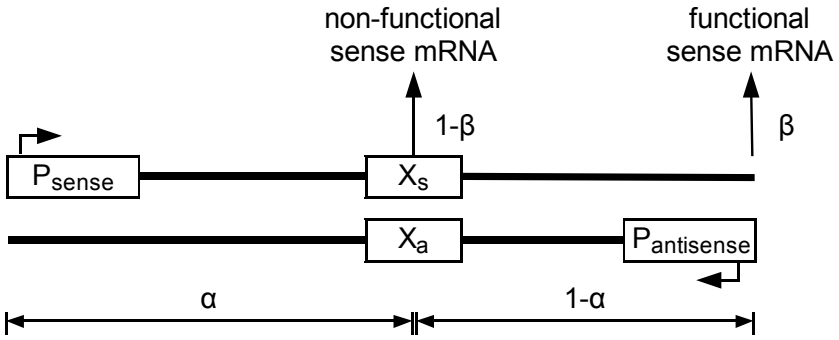

Supplementary Figure 6: Schematic representation of negative interactions between sense and antisense transcription in the refined model. Boxes indicate discrete compartments of DNA, whereas the bold black lines show the two DNA strands. P_{sense} and $P_{antisense}$ refer to sense and antisense promoters, respectively. See text for additional details.

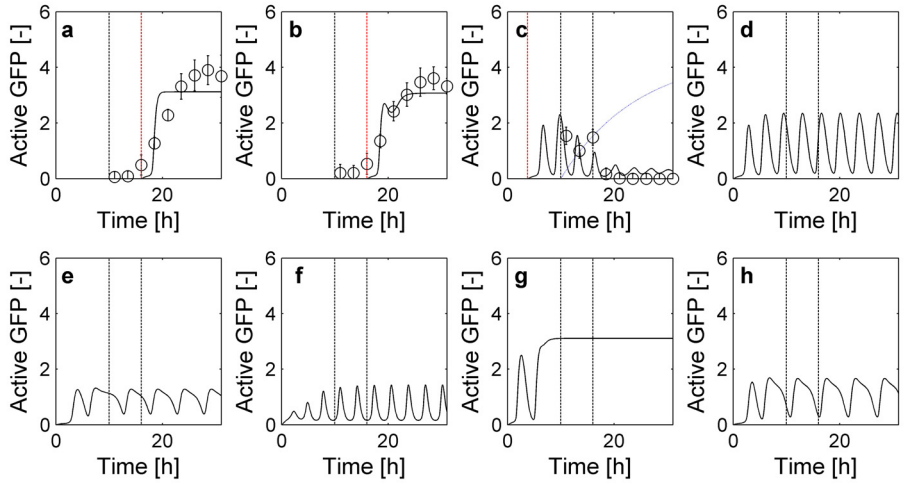

Supplementary Figure 7: Behaviour of the refined model and experimental data used for parameter estimation. (**a**) CHO-K1 co-transfected with pMT35 and pBP282 (1:1; no antibiotics), (**b**) pMT35, pMT36, pBP282 (1:1:1; 200ng/500µl pristinamycin I added 10h after transfection), (**c**) pMT35, pMT36, pBP282 (1:1:1; 1ng/500µl tetracycline added 10h after transfection), (**d**) pMT35, pMT36, pBP282 (1:1:1; no antibiotics; 100ng plasmid DNA), (**e**) pMT35, pMT36, pBP282 (1:1:1; no antibiotics; 50ng plasmid DNA), (**f**) pMT35, pMT36, pBP282 (1:1:1; no antibiotics; 200ng plasmid DNA), (**g**) pMT35, pMT36, pBP282 (2:1:1; no antibiotics; 100ng plasmid DNA), and (**h**) pMT35, pMT36, pBP282 (1:1:1; no antibiotics; 70ng plasmid DNA). In all experiments, cells are transfected with plasmids at t = 0h, antibiotics are added 10h after transfection (left dashed line), and recording of GFP signals starts 16 h after transfection (right dashed line). Solid lines are simulation results for the GFP fluorescence time courses and circles denote selected experimental data used in parameter estimation. Red vertical lines in (**a**)-(**c**) indicate the estimated times of plasmid uptake and the blue dotted line in (**c**) shows the estimated internal tetracycline concentration.

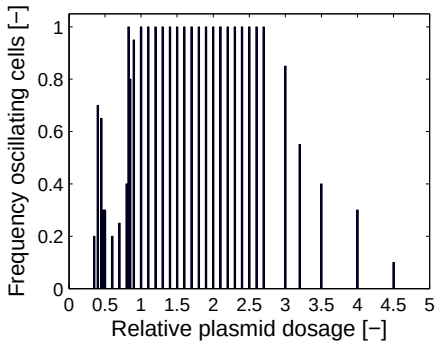

Supplementary Figure 8: Share of oscillating cells as a function of gene dosage as predicted by the stochastic model. In all cases 20 cells with identical initial conditions were simulated; if two or more oscillations were predicted, a simulated cell was counted as oscillatory.

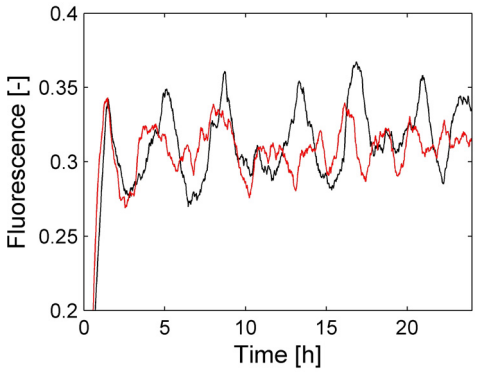

Supplementary Figure 9: Example trajectories for noise-induced oscillations in GFP signals predicted by the stochastic model for relative gene dosages of 3.0 (black) and 3.5 (red). See Fig. 4c,d of the main text for statistical analysis of the results on cell populations.